International Journal of Pharmaceutics 408 (2011) 1–8

Contents lists available at ScienceDirect

International Journal of Pharmaceutics

journal homepage: www.elsevier.com/locate/ijpharm

Mechanical influence of static versus dynamic loadings on parametrical analysis of plasticized ethyl cellulose films

Kangarlou Sogol[a], Haririan Ismaeil[a,b,c,*]

[a] Dept. of Pharmaceutics, School of Pharmacy, Tehran University of Medical Sciences, Tehran, Iran
[b] Biomaterial Research Center (BRC), Tehran University, Tehran, Iran
[c] Medicinal Plants Research Center, Tehran University of Medical Sciences, Tehran, Iran

ARTICLE INFO

Article history:
Received 5 July 2010
Accepted 15 November 2010
Available online 21 November 2010

Keywords:
Ethyl cellulose
Static force
Dynamic force
Michaelis–Menten equation
Lineweaver–Burk equation
Plasticizer

ABSTRACT

The object of this study was to investigate the influence of static and dynamic forces on mechanical properties of the biocompatible polymer ethyl cellulose. Similar polymeric films containing 40% (w/w) of the plasticizer dibutyl sebacate were subjected to tensile forces at different velocities. The average Young's modulus and the variation of yield strength, strain, and strain energy at different velocities complied with the pre-established theories of dynamic loadings. The ultimate strength and the yield strength and/or strain displayed linearity with the velocity, though the ultimate strain and therefore, the plastic and/or ultimate working energies proved non-linear pseudo-Michaelis–Menten behavior. The speculation was that achieving the maximum displacement would probably be the most important cause of failure. Finally the most suitable velocity at which the data would obtain the most demonstrable stress–strain diagrams was selected: tensile forces at almost low velocities, best illustrated as static forces, proved immature failure of the specimens during or shortly after the yield; so that the specimen resembled as a brittle material. High velocities of loadings were also avoided since the strain would usually approach the plateau and would therefore disrupt the rational correlation between forces and displacements during the end region of the curve.

1. Introduction

The object of developing an oral modified release dosage form is to improve the controlled release of the therapeutic agent and thus the drug absorption from the gastrointestinal tract. Such a dosage form effectively reduces the adverse effects associated with peak plasma concentrations beyond the minimum toxic level of the active ingredient while the plasma concentration also maintains within the therapeutic index to achieve the biological effect for a longer period (Sakr, 1999; Streubel et al., 2000; Sood and Panchagnula, 2003; Efentakis and Politis, 2006; Alias et al., 2008; Venkatesh et al., 2008). The dosage form, in particular, controls the amount of drug available for absorption from one dose administration to the next which results in a more stable plasma level of the drug during alternative administration. Targeted drug release in oral administration is achieved through the means of either a release-controlling barrier designed around drug-loaded granules, pellets (Poelvoorde et al., 2008), and/or tablets (Diane Bruce et al., 2008) or employing polymeric or wax systems in formulations (Avgoustakis and Nixon, 1993).

Hence, the primary requirement of these types of dosage forms is their manufacturing process in a reproducible manner so that the drug is delivered at a controlled and consistent rate. The release rate reproducibility, in particular, satisfies the expected therapeutic benefits of the sustained dosage form both in vitro and in vivo. It prevents the detrimental effect of failure of the product following which the dose dumping phenomenon makes the entire drug load of the system being released all at once. In fact, this critical performance of the product has led to the use of coated pellets and/or granules in the development of controlled release dosage forms. Such formulations are generally made up of multiple units with controlled release properties which are either filled into a capsule or compressed into a tablet for ease of administration. The dose is, therefore, divided into several parts and the failure of a few pellets or granules does not seem to significantly impair the performance of the product. The multi-units dosage forms ideally propose a larger margin of safety which substantially resists against premature failure of the system.

When formulating modified release dosage forms, the effects of different in vivo forces, such as the ones due to large mechanical movements and sudden collisions in the alimentary tract should be considered. Moreover, the fluid uptake by the product, which

* Corresponding author at: Dept. of Pharmaceutics, School of Pharmacy, Tehran University of Medical Sciences, P.O. Box 14176-14411, Tehran, Iran.
Tel.: +98 21 66482607; fax: +98 21 66461178.
E-mail address: haririan@tums.ac.ir (H. Ismaeil).

0378-5173/$ – see front matter © 2010 Elsevier B.V. All rights reserved.
doi:10.1016/j.ijpharm.2010.11.031

results in inward production of osmotic stresses and reflection of the forces on internal surface of the core pellet, may also subject the product to microrupturing. The ruptures propagate continuously and dose dumping would eventually happen.

Different classifications of loadings have extensively been defined (Gere and Timoshenko, 1990, pp. 3–6, 81–87; Higdon et al., 1985, pp. 1–59). According to the theories, modified mechanical properties of the structures under time-dependent load exertion are considered as the cornerstone of reproducibility for drug release. Static loadings which are most frequently employed in tensile or compression experiments are defined as gradually increasing loadings while the equilibrium is achieved during a relatively short period of time. Dynamic loads, in comparison, may be applied very suddenly causing vibrations of the structure or they may change in magnitude as time elapses. During the impact loads (also called the energy loads) equilibrium is not established until the vibration is eliminated, usually by natural damping forces. The most basic types of dynamic loads are the impact forces which are commonly produced by the collision of two objects or when a falling solid strikes a structure, and due to cyclical loads typically created by rotating machinery (Gere and Timoshenko, 1990, pp. 9–27, 107–110).

The mechanical theories in static and/or dynamic loadings have largely been simulated in laboratory test profiles. The methodology not only applies to engineering (Al Galib and Limam, 2004; Kim and Kim, 2005; Kolakowski, 2007; Xuand and Wu, 2007; McShane et al., 2008) but has also been repeatedly employed in polymer research (Ging-Ho and Mu-Yuan, 1984; Chen et al., 2002) and analytical techniques to obtain information about biological components in non-destructive manners (Lakos et al., 1995). Clinical analyses were widely used to determine the strength and functional failure of human soft or hard tissues which generally predict the risk of injury in automotive collisions (Pope et al., 1976; Koski and McGill, 1994; Carr et al., 1998; Jacquemoud et al., 2007; Villanueva et al., 2008).

Different structures of polymers nowadays have been examined in formulation of matrix or core-pellets. Matrix pellets with controlled release properties can be produced in a single step, though the prevailing favors turn into the development of coated core-pellets with rate-controlling membranes, the characteristics of which can freely be modulated by simple alteration of the composition and/or thickness of the film coat.

In controlled release drug delivery systems, ethyl cellulose (EC) has been considered as one of the most widely used high molecular weight compounds, which excessively contributes as the water-insoluble compartment of lipophilic coatings. The cellulose ether has also been approved to be capable of being incorporated into majority of other dosage forms as matrices (Crowley et al., 2004), microspheres (Eldridge et al., 1990), and microcapsules (Jalsenjak et al., 19970) or in combination with other cellulose derivatives (Frohoff-Hülsmann et al., 1999; Duarte et al., 2006) and Eudragits (Lecomte et al., 2004; Siepmann et al., 2005).

Considering the widespread application of EC in various dosage forms, an accurate investigation of the polymer mechanics under classical forces may represent an important area in pre-formulation studies. The present study is, therefore, intended to provide a detailed analysis of EC mechanics under static and dynamic loadings.

2. Materials and methods

2.1. Materials and instrumentation

Ethyl cellulose powder was obtained from Dow Chemical Company, USA with an ethoxy content and average viscosity of 48.8% DS and 100 mPs, respectively. Dibutyl sebacate (DBS), with an average density of 0.934–0.945 mg/ml was purchased from Fluka Chemie Gmbh licensed by Sigma–Aldrich Chemie Gmbh (USA; product no. 84840; lot and filling code 447503/1, 21904034). Chloroform, the organic solvent for preparing the sequential polymer solutions, was received from an analytical grade.

The tensile properties of the polymeric films were examined using the universal testing machine of the series Z100 produced by Zwick/Roell group, Germany, employing a 2.0 kN force transducer (load cell) and a pair of 0.5 kN pincer grips. The data were analyzed using the software testXpert V8.1 (copyright© 1995–2000, Zwick Gmbh & Co.).

2.2. Free film preparation

Casting, the most common method ever introduced in numerous literatures, was employed for preparing thin layers of polymer structures. Using a sensitive level vial (bubble tube) with a proper radius of internal curved surface (approximately 20–90-s bubble on a tube with 2-mm divisions), a plane surface was initially leveled (Clarke, 1983). This was done to prohibit the unequal spreading of the polymer solution which results in non-uniform distribution of the thickness in the coalesced polymer along the film. The specimen dimensions, standardized according to both ASTM D882 and ISO 527-1, were equal to 10 and 150 mm for the width and the length of a flat rectangular strip, respectively. The grips were attached to 25 mm from the top and bottom of the strip which restored a gauge length of 100 mm at the beginning of the tension.

To further promote the uniformity of the results, the number of test specimens for each experiment was increased: a cast with an internal area of 15 cm × 30 cm and 2.5 cm depth was prepared out of (float) glass which would provide about 30 similar 10-mm width strips. All the specimens were examined under tension and tensile parameters were recorded among which the data for 10–12 of the specimens with the least variations were selected for final procession of the results. To make a clear observation on the mechanical shifts of the recorded data for both the elastic and plastic regions of the stress–strain diagrams, a typical ductile formulation was selected for uploading the dynamic forces (Kangarlou et al., 2008). This unique sample was prepared by dissolving 3.1 g of the polymer in 100 ml of chloroform and adding the commercial plasticizer DBS to a total 40% (w/w) of the polymer mass.

The mixture was stirred for an hour and left for a further 8–10 h to obtain a more homogeneous state. Prior to use, the solution was again shaken for a few minutes and left for a while to remove the air bubbles. The mixture was then poured into the cast from a distance above the central point and the cast was immediately covered by a piece of nylon sheet which was firmly wrapped around the walls. This would result in practically delayed evaporation of the solvent and would considerably improve the appearance of the upper surface of the film. The cast was left motionless for about 18–20 h, for the solvent to completely dry out, where upon it was semi-filled with cold water. The lateral sides of the rectangular film were carefully separated by means of a surgical blade (code no. 11-1*a*) and then abandoned for a while to allow the water to gradually raise the separated film from the underlying surface of the cast. The sheeting was dried on a blotting paper and reserved at room temperature and relative humidity (23 ± 2 °C and 50 ± 5% RH) for about 72 h prior to the test. Just before the experiment, the length of the polymeric films were divided into 25–30 strips of 10-mm width and the mass and dimensions of the individual specimens were recorded to 0.1 mg and 0.5 mm precision, respectively. A small piece of 20 mm × 5 mm was also separated from each of the films for which the dimensions and mass were similarly measured and its mean thickness was visually determined under a light microscope and 40× objective magnification. The average area and density of the sample were then calculated from the latter data to provide a theoretical means to estimate the mean thickness of each strip in a series of specimens.

Table 1
Tensile parameters for ethyl cellulose plus 40% (w/w) DBS submitted to different loading velocities and accelerations.

Mechanical parameters	Velocity (v) mm/s or acceleration (a) mm/s^2[a]					
	v (or a) 0.05 mm/s^2	v (or a) 0.50 mm/s^2	v (or a) 1.00 mm/^{2}	v (or a) 1.50 mm/s^2	v (or a) 2.00 mm/s^2	v (or a) 3.00 mm/s^2
Thickness ± sd[b] (μm)	97.5 ± 6.4	88.9 ± 3.2	94.8 ± 9.0	88.2 ± 7.3	94.3 ± 5.9	90.8 ± 7.3
Mass ± sd (mg)	131.8 ± 8.6	127.4 ± 4.6	131.1 ± 12.5	127.7 ± 10.6	131.1 ± 8.1	133.5 ± 10.7
E-modulus ± sd (MPa)	214.32 ± 20.13	241.71 ± 12.77	225.50 ± 10.61	213.37 ± 7.97	225.71 ± 7.24	206.98 ± 15.36
σ_{max} ± sd (MPa)	6.15 ± 0.47	9.84 ± 0.36	11.25 ± 0.60	12.74 ± 0.62	14.13 ± 0.49	17.39 ± 1.09
σ_y ± sd (MPa)	6.13 ± 0.47	7.18 ± 0.18	7.65 ± 0.33	7.83 ± 0.16	8.45 ± 0.19	8.94 ± 0.50
ε_B ± sd (%)	14.02 ± 1.32	43.59 ± 3.79	53.42 ± 4.27	63.36 ± 2.66	63.26 ± 3.60	67.85 ± 3.91
ε_y ± sd (%)	6.03 ± 0.46	6.27 ± 0.67	6.46 ± 0.16	7.07 ± 0.19	7.10 ± 0.17	8.27 ± 0.69
U_B ± sd (MJ/m^3)	0.654 ± 0.105	3.313 ± 0.308	4.488 ± 0.416	5.600 ± 0.405	6.150 ± 0.378	7.650 ± 0.676
AUC_e ± sd (MJ/m^3)[c]	0.088 ± 0.012	0.107 ± 0.009	0.130 ± 0.008	0.144 ± 0.004	0.158 ± 0.004	0.193 ± 0.012
AUC_p ± sd (MJ/m^3)[d]	0.566 ± 0.100	3.206 ± 0.304	4.358 ± 0.415	5.456 ± 0.404	5.992 ± 0.377	7.457 ± 0.673
$(AUC_e/AUC_p) \times 100$	15.480	3.326	2.978	2.633	2.640	2.589

[a] Equivalent velocity and acceleration quantities were defined in sequential test series.
[b] Standard deviation measurements were carried out for 12 strips of the sample formula in individual test series.
[c] Elastic $AUC = \sigma_y^2/2E$.
[d] Plastic $AUC = UB - AUC_{elastic.}$

Tensile experiments were conducted at increasing extension speeds (or accelerations) of 0.05, 0.50, 1.00, 1.50, 2.00, and 3.00 mm/s (or mm/s^2), as shown in Table 1. Stress–strain diagrams were drawn and the major tensile parameters (Gere and Timoshenko, 1990, pp. 3–6, 81–87, 9–27, 107–110) for stress and strain values in N/mm^2 or MPa and percent elongations were recorded: σ_y (the yield strength or the stress at the yield point), σ_{max} (maximum tensile strength), σ_B (stress at break), ε_y (yield strain), and ε_B (strain at break) with the Greek letters σ and ε denoting the stress and strain measurements, respectively. The young's modulus or the modulus of elasticity, E (in N/mm^2 or MPa), and the toughness modulus or the energy at break, U_B (in MJ/m^3), were correspondingly recognized in the resilient region based on a tangent model and through the integration of the stress–strain curve from the beginning to the fracture. A further evaluation was done by determining the elastic and plastic strain energies (AUC_{elstic}, $AUC_{plastic}$) based upon the area under the resilient region and subtracting AUC_{elstic} from the total toughness modulus to obtain the plastic surface area, respectively.

2.3. Velocity adjustment experiments—static versus dynamic loadings

To review the theories of impact loading, its mechanics and relevant equations, a round prismatic bar AB is considered (Fig. 1) which is extended longitudinally by the weight force of a single mass, m, transferred through a silk thread[1] of negligible weight to the bottom of the bar (Gere and Timoshenko, 1990, pp. 96–107). The thread is stretched completely and the mass beneath is suspended motionless which results in a static load due to the weight force of the mass m.

During static extension, the load is assumed to be gradually implied as a result of which an instantaneous equilibrium would persist between the force load and the resisting force of the bar. The bar is strained and according to Hookian equations of displacements for axially loaded members, i.e., $\delta = PL/EA$ where P indicates the applied force (Gere and Timoshenko, 1990, pp. 52–55), the maximum elongation of the system following the load exertion is equal to

$$\delta_{st} = \frac{WL}{EA} \quad (1)$$

where δ_{st} is the static elongation of the bar due to the static load W (i.e., the weight force of the mass m). L, E, and A denote respectively, the initial length, elastic Young's modulus, and cross-sectional area of the bar AB where upon the load W is exerted. Comparing to the equilibrium state of forces in the afore-mentioned system, a different condition is explained in which the bar strikes out longitudinally, due to the weight force W, when the suspended m is released from a distance near the bottom of the bar and falls to the maximum affordable extension of the member. The bar is subjected to dynamic loading and the pre-mentioned static equilibrium is temporarily impaired. At the moment of loading, the stress and the elongation are equal to zero. When the load is exerted the resisting force in the bar gradually increases until it equals the weight force W. Once the resistance in the bar equalizes the force W, the elongation of the bar is δ_{st} and the falling mass m obtains a kinetic energy due to the displacement δ_{st}. Hence it continues to move downward until its velocity is again brought to zero by the increasing resistance in the bar. Considering the Hookian force–displacement diagram for the elastic bar AB, when $\delta = \delta_{st}$ the elastic strain energy of the bar, U, is equal to $W\delta_{st}/2$ which is a perfect estimation of the

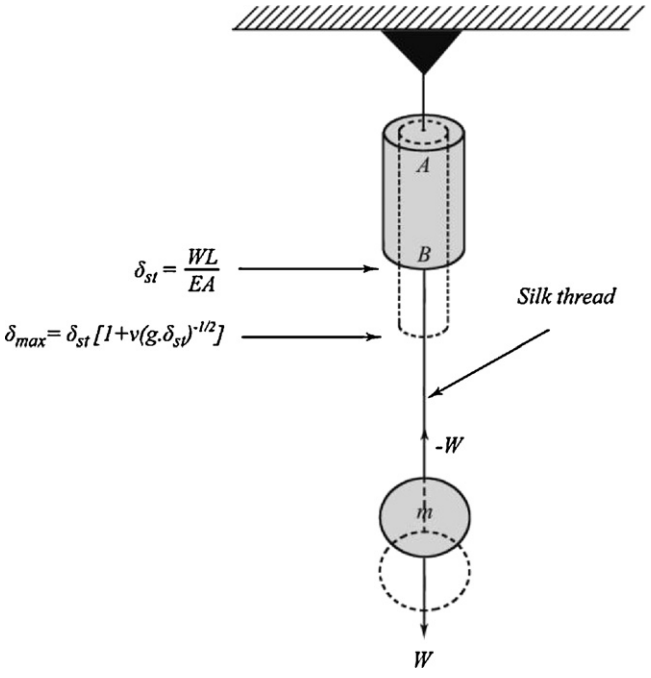

Fig. 1. Schematic diagram for dynamic loadings.

[1] Silk threads are assumed to be strain less and thus, the evaluated strains are merely associated to the extension of the bar AB.

surface area for the resilient triangle in the W–δ_{st} diagram (Gere and Timoshenko, 1990, pp. 88–96).

Substituting the axial weight force W in the previous equation of strain energy with its equivalence from Eq. (1) obtains the concept of toughness strain, $EA\delta_{st}^2/2L$, where $EA/2$ is the stiffness and δ_{st} is the static elongation (Gere and Timoshenko, 1990, pp. 88–96; Higdon et al., 1985, pp. 107–109). The kinetic energy of the falling m is evaluated using $1/2mV^2$ or $WB^2/2g$, where V denotes the instantaneous velocity of the mass m at $\delta = \delta_{st}$. The kinetic energies of the thread and the bar are ignored since they are relatively small when compared to the kinetic energy of the falling object. The potential energy of the falling mass is also determined regarding its lowest position where the bar approaches its greatest elongation δ_{max}. Let δ_1 be the distance the object continues the downward movement after the elongation δ_{st} has been achieved, the extra displacement of the bar due to the potential energy of the falling mass would equal to $\delta_{max} - \delta_{st}$. The potential energy of the object would therefore be equal to $W\delta_1$ or $W(\delta_{max} - \delta_{st})$ and the potential energies of the bar and the thread are likewise disregarded, being negligible compared to that of the object.

Following the above discussion, the total energy of the system at $\delta = \delta_{st}$ is equal to

$$\frac{WV^2}{2g} + W(\delta_{\max} - \delta_{st}) + \frac{EA\delta_{st}^2}{2L} \tag{2}$$

However, when the bar is extended to δ_{max}, the potential energies are disappeared and the velocity of the object decreases to zero which also eliminates the produced kinetic energies in the falling mass. The strain energy of the bar, when it comes into its lowest position is equal to

$$\frac{EA\delta_{\max}^2}{2L} \tag{3}$$

and by using the principle of energy conservation at $\delta = \delta_{st}$ and δ_{max} (i.e., expressions 2 and 3) we obtain

$$\frac{WV^2}{2g} + W(\delta_{\max} - \delta_{st}) + \frac{EA\delta_{st}^2}{2L} = \frac{EA\delta_{\max}^2}{2L} \tag{4}$$

or

$$\frac{WV^2}{2g} + \frac{EA\delta_{st}}{L}(\delta_{\max} - \delta_{st}) = \frac{EA}{2L}(\delta_{\max}^2 - \delta_{st}^2)$$

Further rearrangement of the terms gives:

$$\frac{WV^2}{2g} = \frac{EA}{2L}(\delta_{\max} - \delta_{st})^2$$

Solving this equation for the maximum elongation of the bar leads to:

$$\delta_{\max} = \delta_{st} + \sqrt{\frac{WV^2L}{EAg}} = \delta_{st}\left(1 + \sqrt{\frac{V^2EA}{WLg}}\right) \tag{5}$$

Correspondingly, the maximum strength of the bar is equal to:

$$\sigma_{\max} = \frac{E\delta_{\max}}{L} = \frac{W}{A}\left(1 + \sqrt{\frac{V^2EA}{WLg}}\right) \tag{6}$$

The term in parentheses is called the 'impact factor' which indicates the ratio of maximum elongation to static displacement, and may be many times greater than unity, showing that the dynamic elongation and stress in the bar may be much greater than the corresponding static quantities. It is also obvious from Eqs. (5) and (6) that if $V = 0$, the impact factor is 1 and the expressions obtain the static values as stated before. Thus, increased velocities of loadings produce higher stresses and strains which are similarly characterized according to the theories of dynamic impact loadings.

The preceding analyses are, however, based upon the assumption that no energy loss occurs during impact. In reality, energy loss always occurs during dynamic loading, with most of the energy loss being released in the form of heat or serving as a factor of localized deformation in the structures. Because a great amount of the energy is lost during the experiment, the kinetic energy of the system immediately after the impact is less than it was before the impact, which means that less energy is converted into strain energy in the bar. Therefore, the length of the bar does not displace as much as when energy is conserved. Moreover, to define the mechanics of the impacts, it should also be assumed that the maximum stress in the bar remains within the proportional limit. Beyond the elastic region, the problem becomes more involved because the elongation of the bar is no longer proportional to the axial force. To determine the elongation beyond the yield strain, it usually demands to study a load–displacement diagram of static model where for any assumed maximum elongation δ_1, the strain energy stored in the bar must be equal to the potential energy lost by the system when the object moves to its lowest position at $\delta_{max} = \delta_{st} + \delta_1$. Therefore, when $W(\delta_{st} + \delta_1)$ equals to or is larger than the total area under the curve in the load–displacement diagram, the falling mass will fracture the bar. In some materials, including ductile structures, the stress–strain coordinate of the yield point is raised when the rate of straining of the bar is very large, such as in dynamic loadings, and thus the working energy of dynamic-induced fracture is somewhat higher than the static one. In general, ductile materials offer much greater resistance to impact loads than do brittle materials; the load–displacement curve for a bar of brittle structure displays much smaller area below it than does the curve for a bar of ductile group, even though the ultimate strengths for the two types of materials may be considerably equal.

In the present study, ethyl cellulose films containing an approximate content of 35–45% (w/w) of dibutyl sebacate to the polymer solids would efficiently produce ductile structures (Kangarlou et al., 2008) for the proceeding dynamic experiments.

2.4. Theories of failure

Numerous theories of failure for many types of materials under different contributions of loading have been proposed in mechanical references (Higdon et al., 1985, pp. 487–497). In general, failure of axially loaded members during tension occurs at a specific principal (axial) stress, a definite axial strain, a maximum shearing stress of one-half the axial stress, and a specific amount of strain energy per unit volume of stressed material. Following practical experiences, however, it appears that all the limiting criteria are approached simultaneously and it makes no difference which criterion (stress, strain, or energy) is dominantly used for predicting failure in an axially loaded sample of a material.

For an element subjected to biaxial or triaxial loading, however, the situation is more complicated since the limits of normal stress, normal strain, shearing stress, and strain energy existing at failure for an axial load are not all reached, simultaneously. To determine the best criterion, several theories have been proposed for predicting failure of various types of materials subjected to many combinations of loads. Unfortunately, none of these theories agree with the test data obtained from all types of materials or different combinations of loadings. Several of the more common theories of failure generally presented in numerous references are nevertheless briefly reviewed below.

2.4.1. Maximum-normal-stress theory

The maximum-normal-stress theory predicts failure of a specimen subjected to any combination of loads when the maximum normal stress at any point reaches the axial failure stress σ_f as

determined by an axial tensile or compressive test of the same material.

2.4.2. Maximum-shearing-stress theory

The maximum-shearing-stress theory predicts failure of a specimen subjected to any combination of loads when the maximum shearing stress at any point reaches the failure stress τ_f equal to $\sigma_f/2$, as determined by an axial tensile or compressive test of the same material. For ductile materials the shearing elastic limit (as determined from a torsion test – pure shear) is greater than half the tensile elastic limit (with an average value of τ_f about $0.57\sigma_f$). This means that the maximum-shearing-stress theory errs on the conservative side by being based on the limit obtained from an axial test.

2.4.3. Maximum-normal-strain theory

The maximum-normal-strain theory predicts failure of a specimen subjected to any combination of loads when the maximum normal strain at any point reaches the failure strain σ_f/E at the proportional limit, as determined by an axial tensile or compressive test of the same material.

2.4.4. Maximum-strain-energy theory

The maximum-strain-energy theory predicts failure of a specimen subjected to any combination of loads when the strain energy per unit volume of any portion of the stressed member reaches the failure value of the strain energy per unit volume as determined by an axial tensile or compressive test of the same material. The maximum-strain-energy theory has been largely replaced by the maximum-distortion-energy theory.

2.4.5. Maximum-distortion-energy theory

This theory differs from the maximum-strain-energy theory in that the portion of the strain energy producing volume change is considered ineffective in causing failure by yielding. Supporting evidence comes from experiments showing that homogeneous materials can withstand very high hydrostatic stresses without yielding. The portion of the strain energy producing change of shape of the element is assumed to be completely responsible for the failure of the material by inelastic action.

The strain energy of distortion is most readily computed by determining the total strain energy of the stressed material and subtracting the strain energy corresponding to the volume change.

3. Results

Mean stress–strain diagrams obtained by tensile loading at different velocities (or accelerations) are superimposed in Fig. 2.

The arithmetic mean and the standard deviation of values for mechanical parameters are listed in Table 1. For further prediction of the variation rate of the sequential data for each mechanical parameters at different velocities (or accelerations), functions according to both: (1) the observational data obtained in the real tension and (2) the mathematical interpolations of the values are proposed in Table 2.

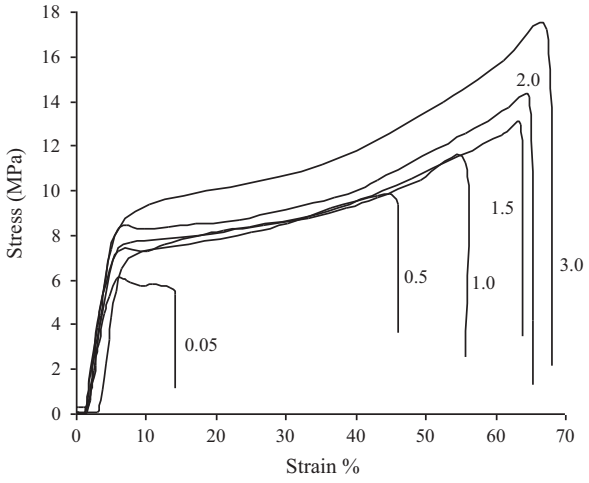

Fig. 2. Median stress–strain diagrams for ethyl cellulose plus 40% (w/w) DBS submitted to different velocities (and accelerations) of loadings.

4. Discussions

Referring to the data presented in Table 1, and considering the rate functions suggested in Table 2, general concepts of dynamism on stress–strain diagrams become apparent. Evidently, the parameter values, in either the resilient region or above the yield point in plastic moiety, indicate sequential increments corresponding to sequential increase in the velocity (v). The recorded Young's modulus for a simple formulation in tensile experiments, however, tends to be rather constant, such as the mean value of 221.28 ± 12.41 MPa at different velocities (or accelerations) in this analysis. It precisely corresponds to both the theoretical Eq. (6) described in Section 2.3 and the practical zero-order rate function proposed in Table 2. As previously explained in Eqs. (5) and (6) for the maximum elastic displacement and strength in dynamic loadings, the values of yield strength (σ_y), yield strain (ε_f) and the resilient work load (the elastic surface area or AUC_e) acquire linearly increasing quantities with the increase in the velocity. This apparently demonstrates the correlation of the pre-established theories of dynamism below the yield point and the practical observations of the first-order rate functions proposed for the mentioned parameters in Table 2.

In the plastic region of the stress–strain diagram, beyond the yield point, the suggested equations and theories in dynamic

Table 2
Non-linear inter-specimen variation functions for mechanical parameters up to yield and break points obtained under different velocities and accelerations.

Variation functions	Mechanical parameters			
	E-modulus (MPa)	σ_y (MPa)	ε_y (%)	AUC_e (MJ/m^3)
Order (theorized and/or observational)	Zero	First	First	First
$y = f(x)$[a]	$y = 221.277$	$y = 0.886x + 6.508$	$y = 0.743x + 5.870$	$y = 0.035x + 0.090$
R-squared value (R^2)	–	$R^2 = 0.92248$	$R^2 = 0.95698$	$R^2 = 0.99327$

Variation functions	Mechanical parameters			
	σ_{max} (MPa)	ε_B (%)	AUC_p (MJ/m^3)	U_B (MJ/m^3)
Order (observational)	First	Michaelis and Menten	Michaelis and Menten	Michaelis and Menten
$y = f(x)$[a]	$y = 3.523x + 7.190$	$1/y = 0.003(1/x) + 0.015$	$1/y = 0.082(1/x) + 0.131$	$1/y = 0.070(1/x) + 0.136$
R-squared value (R^2)	$R^2 = 0.96227$	$R^2 = 0.99629$	$R^2 = 0.99942$	$R^2 = 0.99874$

[a] y and x denote for the distinct mechanical parameter and the velocity (v), respectively.

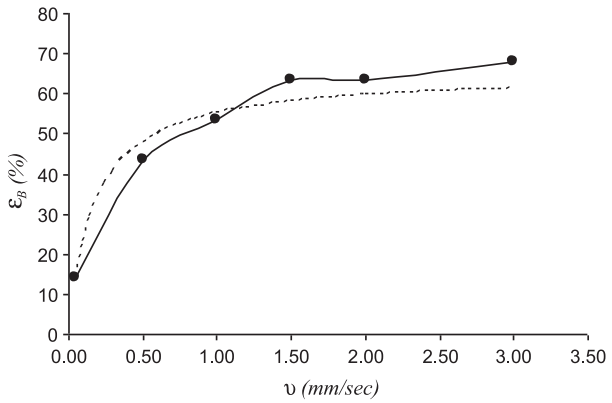

Fig. 3. Ultimate strain (ε_B)–velocity (v) diagram. Solid line, experimental curve; dashed line, interpolated curve of the equation $(\varepsilon_B)_i = (\varepsilon_B)^{ave}_{max} \cdot v/(v + k_\varepsilon)$ in the velocity range of 0.05–3 mm/s, considering the average of the three latest maximum experimental ε_B s ($(\varepsilon_B)^{ave}_{max} = 64.82$) as the maximum tolerable strain and the relating velocity to ($(\varepsilon_B)^{ave}_{max}/2 (\cong 0.18)$) as the approximate k_ε of the mentioned equation.

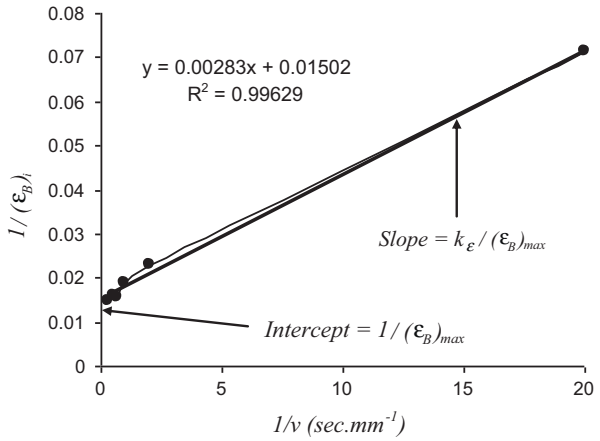

Fig. 4. The pseudo-Lineweaver–Burk plot for the inverted ultimate strain ($1/(\varepsilon_B)_i$)–velocity ($1/v$) diagram.

impact loadings would no longer comply with practice. Nevertheless, the observations for the ultimate strength (σ_{max}) in Table 1 tend to display a roughly linear progression with the gradual increase in the velocity. This supports the evidences of a first-order rate function with a slope of about 4-fold greater than the slope of variation in v-yield strength function.

Referring to the recorded values for the maximum strain up to break (Table 1), surprisingly, more complicated functions seem to be able to demonstrate the ε_B variation. A detailed investigation of total displacement at failure represents first-order variation of strain quantities when the loading velocity remains at rather minimal values followed by zero-order plateau-like rate function when loading attains higher velocities. In other words, the ultimate strains of the sample EC formula in stress–strain diagrams display a dual function at low and high velocities of tension: at rather low speeds of loading, the ultimate strain tends to increase linearly with sequential increase in the velocity; whereas higher speeds of impact result in the maximum strains of the polymer composite to be approached (Higdon et al., 1985, pp. 487–497) which also point out the almost unchanged values of displacement or trivial fluctuations of the strain during tension.

A plot of the recorded data for ε_B against the speed of loading (Fig. 3) reminds the kinetics of single-substrate enzyme catalyzed reactions. The hyperbolic relationship between initial velocity (v_0) and initial substrate concentration ($[S_0]$) is expressed by the universal Michaelis–Menten equation:

$$v_0 = \frac{v_{max} \cdot [S_0]}{[S_0] + k_m} \tag{7}$$

where v_{max} is the maximum v_0 at a particular total enzyme concentration and k_m theoretically equals the value of $[S_0]$ which gives an initial velocity equal to $1/2 v_{max}$ (Michaelis and Menten, 1913; Cha, 1968; Ricard and Cornish-Bowden, 1987; Hammes, 2002; Cleland, 2005).

Considering the Michaelis–Menten relationship and substituting the mechanical parameters $(\varepsilon_B)_i$, $(\varepsilon_B)_{max}$, and v for the respective values of v_0, v_{max}, and $[S_0]$ in Eq. (7) obtains

$$(\varepsilon_B)_i = \frac{(\varepsilon_B)_{max} \cdot v}{v + k_\varepsilon} \tag{8}$$

in which $(\varepsilon_B)_i$ and $(\varepsilon_B)_{max}$ are the instant ultimate strain of the composite at different speeds and the maximum tolerable strain at rather high velocities in a pseudo-Michaelis–Menten phenomenon, respectively. k_ε preserves the same meaning as k_m and represents the velocity at which the sample fails with half of its natural tolerable strain. Theoretically, when the velocity remains at rather low values, the parameter v is ignored with respect to k_ε in the denominator, providing a first-order relationship between the strain and velocity. This means that the function of strain changes complies rather completely with the increase in the speed of loading (Eq. (8.1)). However, when the speed is maximized, the rather small quantities of k_ε are neglected with respect to the great values of v and the failure occurs at the maximum possible displacement of the specimen (Eq. (8.2)).

$$(\varepsilon_B)_i = \frac{(\varepsilon_B)_{max}}{k_\varepsilon} \cdot v \tag{8.1}$$

$$(\varepsilon_B)_i = (\varepsilon_B)_{max} \tag{8.2}$$

Unfortunately, the graph of the pseudo-Michaelis–Menten equation does not provide the satisfactory means for determining $(\varepsilon_B)_{max}$ and k_ε; the ultimate strain approaches the real maximum tolerable strain in tangential fashion, only actually attaining it, when the impact loadings are implied at infinitely large velocities. The observed hyperbola therefore, cannot be accurately extrapolated outwards since the recorded values of strain at break at different velocities are strictly limited to loading speeds lower than the upper threshold for the maximum tensile velocity available in the instrument.

To overcome the problem, the pseudo-Michaelis–Menten Eq. (8) was simply transformed taking advantage of the Lineweaver–Burk inversion plots (Lineweaver and Burk, 1934; Greco and Hakala, 1979; Emaduddin and Takeuchi, 1996):

$$\frac{1}{(\varepsilon_B)_i} = \frac{v + k_\varepsilon}{(\varepsilon_B)_{max} \cdot v} = \frac{v}{(\varepsilon_B)_{max} \cdot v} + \frac{k_\varepsilon}{(\varepsilon_B)_{max} \cdot v}$$

$$\frac{1}{(\varepsilon_B)_i} = \frac{k_\varepsilon}{(\varepsilon_B)_{max}} \cdot \frac{1}{v} + \frac{1}{(\varepsilon_B)_{max}} \tag{9}$$

This is of the form $y = mx + c$, which is the equation of a straight line with a slope of $m = k_\varepsilon/(\varepsilon_B)_{max}$ and the intercept of $c = 1/(\varepsilon_B)_{max}$ along $1/(\varepsilon_B)_i$, i.e., the inverse ultimate strain axis (Fig. 4).

The pseudo-Lineweaver–Burk rate function (Table 2) can easily be extrapolated to tension speeds higher than the maximum affordable velocity threshold of load exertion. Thus, the inverse rearrangement practically promotes the precision of estimations for the maximum tolerable strain quantities in the polymer specimen.

Further procession of the data for plastic working energies at different velocities (Table 1), suggests a pseudo-Michaelis–Menten hyperbolic relationship where in the substitution of ε_B and k_ε by

comparative parameters AUC_p and k_A, respectively, obtains

$$(AUC_p)_i = \frac{(AUC_p)_{\max} \cdot v}{v + k_A} \quad (10)$$

Similarly $(AUC_p)_i$ and $(AUC_p)_{max}$ express the instant plastic strain energy at different loading speeds and the maximum distinguished plastic toughness modulus at approximately very high velocities, respectively. k_A resembles the constant k_ε and indicates the velocity at which $(AUC_p)_i = 1/2(AUC_p)_{max}$. The pseudo-Lineweaver–Burk rate function has also been calculated in Table 2 from which the extrapolating constants $(AUC_p)_{max}$ and k_A can fairly be recognized.

The total strain energy U_B, which simultaneously reflects the effects of a conjugation between the first-order variation in AUC_e and the mixed zero- and first-order variation in AUC_p, results in a similar pseudo-Michaelis–Menten relationship where the replacement of ε_B and k_ε with U_B and k_U, respectively, obtains

$$(U_B)_i = \frac{(U_B)_{\max} \cdot v}{v + k_U} \quad (11)$$

$(U_B)_i$, $(U_B)_{max}$, and k_U in the previous equation explain the instant strain energy at break at different velocities, the maximum achievable strain energy at break at infinitely high velocities of loadings, and the loading velocity at which the polymer network obtains half of its maximum achievable toughness, respectively. The inverse rearrangement of the fraction in Eq. (11) obtains the pseudo-Lineweaver–Burk function (Table 2), which perceptively points out the effectiveness of a mixed zero- and first-order function for toughness variation at different velocities.

To decide about the most appropriate velocity at which tensile experiments are suggestively performed, a proportionate quantity was derived which express the percent values of the elastic surface area (AUC_e) divided by the plastic surface moiety (AUC_p). This parameter declares the fractions of strain energy modules at various loading velocities (Table 1). Referring to the mean stress–strain diagrams superimposed in Fig. 2 and considering the sequential variations of the *AUC*s ratio in Table 1, it is obvious that static forces at very low tensile speeds (i.e., $v = 0.05$ mm/s) result in almost defective force–displacement curves due to immature failure of the product. The resilient characteristics of the matter therefore, dominate which resemble a very weak and brittle feature of the structure. In contrast to static forces at low velocities, dynamic impact loadings at maximum tensile speeds (i.e., $v = 1.5$, 2, and 3 mm/s in the present assay) results in the maximum tolerable strain (and/or plastic strain energy) to be achieved. The maximum strain results in an evident plateau-like displacement in the end region of the force–displacement curve which would no longer express the rational correlation between the constant values of ultimate strain with the increasing strength at high velocities. The maximum elongation and/or plastic strain energy or toughness would deductively be in charge of the most probable cause of specimen failure (refer to part 2.4 for theories of failure and Higdon et al., 1985, pp. 487–497) and would clearly excludes the usefulness of high loading velocities (i.e., dynamic impact loadings) in tensile experiments.

Comparing to low velocities, the stress–strain diagram at medium loading speeds (i.e., $v = 0.5$ to 1 mm/s in the present experiment), attribute more extended areas to both elastic and plastic moieties. This is particularly useful when the resilient and toughness quantities of different polymer formulations are intended to be compared in mechanical analyses. In contrast to high velocities, the individual coordinates in the stress–strain diagrams at medium tension speeds concern a perceptively meaningful correlation of the spontaneous stresses and strains during the whole period of loading from the beginning to the failure. The delay at speed switching, comparable to acceleration constant in the initial lag period of load exertion, likewise may be settled within the similar range of velocity. As a result the constant speed of tension approaches in less than about 1 or 2 s.

The theories and practice of speed regulation discussed in this trial is exclusively applicable for simulative experiments performed on EC-plasticized structures. Nevertheless the general concepts and statements of static versus dynamic impact loadings still properly corroborate the practical observations in various polymeric and inorganic specimens. To discover the most appropriate loading velocity and acceleration limits for various specimens, however, discriminative experiments should be primarily performed and the fundamentals in each analysis should be based on the exclusive information obtained from stress–strain diagrams at different loading speeds.

References

Al Galib, D., Limam, A., 2004. Experimental and numerical investigation of static and dynamic axial crushing of circular aluminum tubes. Thin-Walled Struct. 42, 1103–1137.

Alias, J., Silva, I., Goñi, I., Gurruchaga, M., 2008. Hydrophilic amylose-based graft copolymers for controlled protein release. Carbohydr. Polym. 74, 31–40.

Avgoustakis, K., Nixon, J.R., 1993. Biodegradable controlled release tablets. II. Preparation and properties of poly(lactide-co-glycolide) powders. Int. J. Pharm. 99, 239–246.

Carr, R.W., Gregory, J.E., Proske, U., 1998. Summation of responses of cat muscle spindles to combined static and dynamic fusimotor stimulation. Brain Res. 800, 97–104.

Cha, S., 1968. A simple method for derivation of rate equations for enzyme-catalyzed reactions under the rapid equilibrium assumption or combined assumptions of equilibrium and steady state. J. Biol. Chem. 243, 820–825.

Chen, W., Lu, F., Cheng, M., 2002. Tension and compression tests of two polymers under quasi-static and dynamic loading. Polym. Test. 21, 113–121.

Clarke, L.D. (Ed.), 1983. Plane and Geodetic Surveying for Engineers – Plane Surveying, vol. 1, 6th ed. CBS Publishers & Distributors, Delhi, pp. 33–37.

Cleland, W.W., 2005. The use of isotope effects to determine enzyme mechanisms. Arch. Biochem. Biophys. 433, 2–12.

Crowley, M.M., Schroeder, B., Fredersdorf, A., Obara, S., Talarico, M., Kucera, S., McGinity, J.W., 2004. Physico-chemical properties and mechanism of drug release from ethyl cellulose matrix tablets prepared by direct compression and hot-melt extrusion. Int. J. Pharm. 269, 509–522.

Diane Bruce, L., Shah, N.H., Waseem Malick, A., Infeld, M.H., McGinity, J.W., 2008. Properties of hot-melt extruded tablet formulations for the colonic delivery of 5-aminosalicylic acid. Eur. J. Pharm. Biopharm. 59, 85–97.

Duarte, A.C., Gordillo, M.D., Cardoso, M.M., Simplicio, A.L., Duarte, C.M.M., 2006. Preparation of ethyl cellulose/methyl cellulose blends by super critical antisolvent precipitation. Int. J. Pharm. 311, 50–54.

Efentakis, M., Politis, S., 2006. Comparative evaluation of various structures in polymer controlled drug delivery systems and the effect of their morphology and characteristics on drug release. Eur. Polym. J. 42, 1183–1195.

Eldridge, J.H., Hammond, C.J., Meulbroek, J.A., Staas, J.K., Gilley, R.M., Tice, T.R., 1990. Controlled vaccine release in the gut-associated lymphoid tissues. Part I. Orally administered biodegradable microspheres target the Peyer's patches. J. Control. Release 11, 205–214.

Emaduddin, M., Takeuchi, H., 1996. Lineweaver–Burk analysis for the blocking effects of mammalian dopamine receptor antagonists on dopamine-induced currents in achatina giant neurones. Gen. Pharmacol. 27, 1209–1213.

Frohoff-Hülsmann, M.A., Schmitz, A., Lippold, B.C., 1999. Aqueous ethyl cellulose dispersions containing plasticizers of different water solubility and hydroxypropyl methyl cellulose as coating material for diffusion pellets. Part I: drug release rates from coated pellets. Int. J. Pharm. 177, 69–82.

Gere, J.M., Timoshenko, S.P. (Eds.), 1990. Mechanics of Materials. , 3rd ed. PWS-KENT Publishing Company, Boston (a) pp. 3–6, 81–87, (b) pp. 9–27, 107–110, (c) pp. 96–107, (d) pp. 52–55, and (e) pp. 88–96.

Ging-Ho, H., Mu-Yuan, M.M., 1984. Dynamic and static properties of SBS triblock copolymer and their blends. Polymer 25, 882–889.

Greco, W.R., Hakala, M.T., 1979. Evaluation of methods for estimating the dissociation constant of tight binding enzyme inhibitors. J. Biol. Chem. 254, 12104–12109.

Hammes, G., 2002. Multiple conformational changes in enzyme catalysis. Biochemistry 41, 8221–8228.

Higdon, A., Ohlsen, E.H., Stiles, W.B., Weese, J.A., Riley, W.F. (Eds.), 1985. Mechanics of Materials. , 4th ed. John Wiely & Sons, New York (a) pp. 1–59, (b) pp. 107–109, and (c) pp. 487–497.

Jacquemoud, C., Bruyere-Garnier, K., Coret, M., 2007. Methodology to determine failure characteristics of planar soft tissues using a dynamic tensile test. J. Biomech. 40, 468–475.

Jalsenjak, I., Nicolaidou, C.F., Nixon, J.R., 1997. Dissolution from tablets prepared using ethyl cellulose microcapsules. J. Pharm. Pharmacol. 29, 169–172.

Kangarlou, S., Haririan, I., Gholipour, Y., 2008. Physico-mechanical analysis of free ethyl cellulose films comprised with novel plasticizers of vitamin resources. Int. J. Pharm. 356, 153–166.

Kim, N.-I.L., Kim, M.-Y., 2005. Exact dynamic/static stiffness matrices of non-symmetric thin-walled beams considering coupled shear deformation effects. Thin-Walled Struct. 43, 701–734.
Kolakowski, Z., 2007. Some aspects of dynamic interactive buckling of composite columns. Thin-Walled Struct. 45, 866–871.
Koski, A.V., McGill, S.M., 1994. Dynamic shoulder flexion strength: for use in occupational risk analysis and clinical assessment. Clin. Biomech. 9, 99–104.
Lakos, Z., Szarka, Á., Koszorús, L., Somogyi, B., 1995. Quenching-resolved emission anisotropy: a steady state fluorescence method to study protein dynamics. J. Photochem. Photobiol. B: Biol. 27, 55–60.
Lecomte, F., Siepmann, J., Walther, M., MacRae, R.J., Bodmeier, R., 2004. Polymer blends used for the aqueous coating of solid dosage forms: importance of the type of plasticizer. J. Control. Release 99, 1–13.
Lineweaver, H., Burk, D., 1934. The determination of enzyme dissociation constants. J. Am. Chem. Soc. 56, 658–666.
McShane, G.J., Stewart, C., Aronson, M.T., Wadley, H.N.G., Fleck, N.A., Deshpande, V.S., 2008. Dynamic rupture of polymer–metal bilayer plates. Int. J. Solids Struct. 45, 4407–4426.
Michaelis, L., Menten, M., 1913. Die Kinetik der Invertinwirkung. Biochem. Z. 49, 333–369.
Poelvoorde, N., Huyghebaert, N., Vervaet, C., Remon, J.P., 2008. Optimisation of an enteric coated, layered multi-particulate formulation for ileal delivery of viable recombinant *Lactococcus lactis*. Eur. J. Pharm. Biopharm. 69, 969–976.
Pope, M.H., Crowninshield, R., Miller, R., Johnson, R., 1976. The static and dynamic behavior of the human knee in vivo. J. Biomech. 9, 449–452.
Ricard, J., Cornish-Bowden, A., 1987. Co-operative and allosteric enzymes: 20 years on. Eur. J. Biochem. 166, 255–272.
Sakr, F.M., 1999. A programmable drug delivery system for oral administration. Int. J. Pharm. 184, 131–139.
Siepmann, F., Siepmann, J., Walther, M., MacRae, R.J., Bodmeier, R., 2005. Blends of aqueous polymer dispersions used for pellet coating: importance of particle size. J. Control. Release 105, 226–239.
Sood, A., Panchagnula, R., 2003. Design of controlled release delivery systems using a modified pharmacokinetic approach: a case study for drugs having a short elimination half-life and a narrow therapeutic index. Int. J. Pharm. 261, 27–41.
Streubel, A., Siepmann, J., Peppas, N.A., Bodmeier, R., 2000. Bimodal drug release achieved with multi-layer matrix tablets: transport mechanisms and device design. J. Control. Release 69, 455–468.
Venkatesh, S., Saha, J., Pass, S., Byrne, M.B., 2008. Transport and structural analysis of molecular imprinted hydrogels for controlled drug delivery. Eur. J. Pharm. Biopharm. 69, 852–860.
Villanueva, I., Hauschulz, D.S., Mejic, D., Bryant, S.J., 2008. Static and dynamic compressive strains influence nitric oxide production and chondrocyte bioactivity when encapsulated in PEG hydrogels of different crosslinking densities. Osteoarthritis Cartilage 16, 909–918.
Xuand, R., Wu, Y., 2007. Static, dynamic, and buckling analysis of partial interaction composite members using Timoshenko's beam theory. Int. J. Mech. Sci. 49, 1139–1155.